PREMIUM JET COOLING WITH TWO RIBS OVER FLAT PLATE UTILIZING NANOFLUID MIXED CONVECTION

by

Wael El-MAGHLANY[a], Mohamed TEAMAH[a,b], A. E. KABEEL[c] *, and Ahmed A. HANAFY[b]

[a]Faculty of Engineering, Alexandria University, Alexandria, Egypt
[b]Arab Academy for Science and Technology and Maritime Transport, Alexandria, Egypt
[c]Faculty of Engineering, Tanta University, Tanta, Egypt

Original scientific paper
https://doi.org/10.2298/TSCI141228056E

In this study, a numerical simulation of the thermal performance of two ribs mounted over a horizontal flat plate and cooled by Cu-water nanofluid is performed. The plate is heated and maintained at a constant temperature and cooled by mixed convection of laminar flow at a relatively low temperature. The top wall is considered as an adiabatic condition. The effects of related parameters such as Richardson number ($0.01 \le Ri \le 10$), the solid volume fraction ($0.01 \le \phi \le 0.06$), the distance ratio between the two ribs ($d/W = 5$, 10, and 15), and the rib height ratio ($b/W = 1$, 2, and 3) on the ribs thermal performance are studied. The numerical simulation results indicate that the heat transfer rate is significantly affected by the distance and the rib height. The heat transfer rate is improved by increasing the nanoparticles volume fraction. The influence of the solid volume fraction with the increase of heat transfer is more noticeable for lower values of the Richardson number. The numerical results are summarized in the effect of pertinent parameters on the average Nusselt number with the assistance of both streamlines and isothermal ones. Throughout the study, the Grashof and Prandtl numbers, for pure water are kept constant at 10^3 and 6.2, respectively. The numerical work was displayed out using, an in-house computational fluid dynamic code written in FORTRAN, which discretizes non-dimensional forms of the governing equations using the finite volume method and solves the resulting system of equations using Gauss-Seidal method utilizing a tri diagonal matrix algorithm.

Key words: *nanofluid, mixed convection, rib, jet cooling*

Introduction

Many industries need an efficient method for cooling; using jet impingement is an attractive cooling process due to its capability of achieving a high-heat transfer rate. In some applications such as laser or plasma cutting processes, the jet impingement cooling can reduce thermal deformation of products. Maghrebi *et al.* [1] investigated the effects of nanoparticle volume fraction in hydrodynamic and thermal characteristics of an incompressible forced 2-D plane jet flow. Abdel-Fattah [2] carried out numerically and experimentally an investigation for impinging circular twin-jet flow with no cross-flow, his study was performed for high Reynolds number values. Confined impinging the air jet at moderately low Reynolds numbers was investigated experimentally by Baydar [3], the study was performed for both single and double jets. Baydar and Ozmen [4] studied both experimentally and numerically the flow field and heat

* Corresponding author, e-mail: kabeel6@hotmail.com

transfer of a confined impinging air jet at high Reynolds numbers, the flow was turbulent , the effect of both Reynolds number and jet to plat space was examined. Cavadas *et al.* [5] carried out numerically and experimentally for both Newtonian and non-Newtonian fluids the laminar impinging jet flow confined by sloping plane walls. Thermal performance of two types of both confined and unconfined impinging jets was performed by Choo and Kim [6]. Their study was performed for both air and water, the investigated parameters were the dimensionless pumping powers and jet to plat spacing. Guerra *et al.* [7] studied the behavior of velocity and temperature due to turbulent impinging jet by scaling log-laws. Owing to the increase in temperature differences between the jet and the target plate from confined impinging jets; the natural convection effect is remarkable, this effect was studied by Koseoglu and Baskaya [8], both jet-to-plate spacing and Reynolds number effect was investigated. Lee *et al.* [9] introduced the different unsteadiness that developed within confined impinging slot jets. The study was performed for laminar impinging slot jets. Lee *et al.* [10] presented the effect of both Reynolds number and different channel spacing numerically. The impact of nanoparticles on the enhancement of heat transfer for confined and submerged impinging jet was performed experimentally by Nguyen *et al.* [11], it has been detected that nanofluids with high particle volume fractions not appropriate for the heat transfer enhancement purpose under the confined impinging jet configuration. Ozmen [12] carried out experimentally confined twin jets resulting from the lower surface and impinging normally on the upper surface. San and Chen [13] studied for multiple numbers of jets the Nusselt number variation on a flat surface; the study was performed experimentally. San and Shiao [14] examined for heat flux conditions the effects of jet plate size and plate spacing on the heat transfer characteristics of a confined circular air jet impinging on a flat plate. Yousefi-Lafouraki *et al.* [15] studied numerically laminar forced convection in a confined slot impinging jet; the channel was in convergent shape, effect of different geometrical parameters and the Reynolds number values have been introduced. The thermal performance of confined impinging slot jet with air as a working fluid was studied by Zukowski [16], effect of nozzle width, Reynolds number, and nozzle to plate spacing on the Nusselt number was investigated. Behnia *et al.* [17] simulated the heat transfer and flow in circular confined and unconfined impinging jet arrangements numerically; the study was performed for turbulent flow regions. Beitelmal *et al.* [18] studied the effect of the jet inclination angles on the heat transfer between a flat surface and an impinging two-dimensional jet with the air as a working fluid experimentally. The turbulent flow over moving flat surface due to slot air jet impinging on a moving flat surface was investigated by Senter and Solliec [19]. Yan and Saniei [20] studied the local convective heat transfer coefficients over flat plate due to impinging circular air jet experimentally; the jet was oblique, and the oblique angles were changed. Dagtekin and Oztop [21] investigated numerical heat transfer due to double impinging laminar slow jet within the one side closed long duct. It was found that the mean Nusselt number increases almost linearly with increasing of Reynolds number. Most of the researchers mentioned above considered the heat transfer enhancement by: changing the number of jets, the jet to plate spacing, the cooling fluid type or by adding nanofluids. This study concerned with 2-D water jet from a slot and impinging on a heated flat plate. The primary objective of this study is to examine the effect of both rib and nanofluids on the heat transfer performance. As such, the cooling of hot horizontal plate with two mounted ribs by a water Cu nanofluid is investigated in this paper.

Mathematical formulation

A schematic of the system under consideration is shown in fig. 1, the horizontal hot plate with ribs and confined upper, insulated plate. The confined upper, insulated plate has

only one single cooling jetport, both left-hand side and the right-hand side ends (of the formed duct with the horizontal hot plate with ribs and confined upper, insulated plate) are open to allow the flow to escape. To simulate the confined fluid jet impingement system, some geometrical parameters are introduced in the figure. The plate length is long enough to satisfy fully developed flow exit conditions (L = 40 W). The following dimensions (only as simulated parameters) as a function of the entrance port width are: $a/W = 1$, $H/W = 4$, $b/W = 1$, 2, and 3, while $d/W = 5$, 10, and 15, respectively, the only changed parameters were; rib to rib spacing (D) and rib height (b) and their effect on heat transfer, which are the objective of this study.

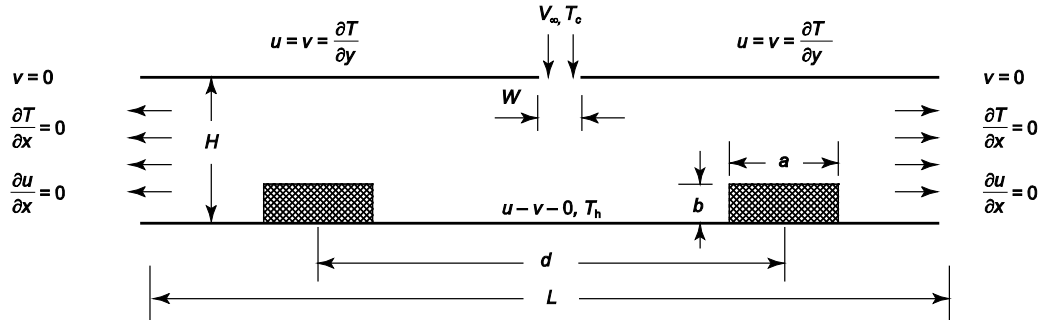

Figure 1. The schematic diagram for the problem with boundary conditions

The nanofluid contains water, and Cu nanoparticles are in thermal equilibrium with physical properties as listed in tab. 1. The Cu nanoparticles are assumed to be spherical in uniform shape and size. The nanofluid is Newtonian and incompressible, whereas the flow is laminar, and radiation effects are negligible. Constant thermophysical properties are considered for the nanofluid, except for the density variation in the buoyancy forces that are determined to the Boussinesq approximation. The properties of the nanofluids are given by the following.

Table 1. Thermophysical properties of pure water and nanoparticles

Physical properties	ρ [kgm^{-3}]	C_p [Jkg^{-1}K^{-1}]	k [Wm^{-1}K^{-1}]	β [K^{-1}]
Pure water	997.1	4179	0.613	$21 \cdot 10^{-5}$
Cu	8933	385	400	$1.67 \cdot 10^{-5}$

The effective density of the nanofluid is:

$$\rho_{\mathrm{nf}} = (1 - \varphi)\rho_{\mathrm{f}} + \varphi\rho_s \tag{1}$$

The effective dynamic viscosity of the nanofluid given by Brinkman [22] is:

$$\mu_{\mathrm{nf}} = \frac{\mu_{\mathrm{f}}}{(1-\varphi)^{2.5}} \tag{2}$$

The thermal diffusivity of the nanofluid is:

$$\alpha_{\mathrm{nf}} = \frac{k_{\mathrm{nf}}}{(\rho C_p)_{\mathrm{nf}}} \tag{3}$$

The heat capacitance of the nanofluid is:

$$(\rho C_p)_{\mathrm{nf}} = (1 - \varphi)\,(\rho C_p)_{\mathrm{f}} + \varphi(\rho C_p)_s \tag{4}$$

The thermal expansion coefficient is:

$$(\rho\beta)_{\mathrm{nf}} = (1-\varphi)\,(\rho\beta)_{\mathrm{f}} + \varphi(\rho\beta)_s \tag{5}$$

The effective thermal conductivity of the nanofluid is determined using the model proposed by Patel *et al.* [23]. For this two-component entity of spherical particle suspension, the model gives:

$$k_{\mathrm{nf}} = k_{\mathrm{f}}\left[1+\frac{k_s}{k_{\mathrm{f}}}\frac{d_{\mathrm{f}}\varphi}{d_s(1-\varphi)}+\sigma\,\mathrm{Pe}\,\frac{d_{\mathrm{f}}\varphi}{d_s(1-\varphi)}\frac{k_s}{k_{\mathrm{f}}}\right] \tag{6}$$

where k_s and k_{f} are the thermal conductivities of dispersed Cu nanoparticles and pure water. The experimental constant is σ = 36000 as suggested by Santra *et al.* [24] for a water-Cu nanofluid.

The diameter of solid nanoparticles is d_s = 100 nm, and the molecular size of the base fluid is d_{f} = 2 Å.

$$\mathrm{Pe} = \frac{d_s}{\alpha_{\mathrm{f}}}\frac{2\Gamma_b T}{\pi\mu_{\mathrm{f}}d_s^2} \tag{7}$$

where $(2\Gamma_b T/\pi\mu_{\mathrm{f}}d_s^{\,2})$ is the nanoparticles Brownian motion velocity, and $\Gamma_b = 1.3807\cdot10^{-23}$ J/K is the Boltzmann constant.

With the previous assumptions, the non-dimensional governing equations of continuity, momentum and energy for nanofluid are:

$$\frac{\partial U}{\partial X}+\frac{\partial V}{\partial Y}=0 \tag{8}$$

$$U\frac{\partial U}{\partial X}+V\frac{\partial U}{\partial Y}=-\frac{\partial P}{\partial X}+\frac{\mu_{\mathrm{nf}}\rho_{\mathrm{f}}}{\mu_{\mathrm{f}}\rho_{\mathrm{nf}}}\frac{\lambda}{\mathrm{Re}}\left(\frac{\partial^2 U}{\partial X^2}+\frac{\partial^2 U}{\partial Y^2}\right) \tag{9}$$

$$U\frac{\partial V}{\partial X}+V\frac{\partial V}{\partial Y}=-\frac{\partial P}{\partial Y}+\frac{\mu_{\mathrm{nf}}\rho_{\mathrm{f}}}{\mu_{\mathrm{f}}\rho_{\mathrm{nf}}}\frac{\lambda}{\mathrm{Re}}\left(\frac{\partial^2 V}{\partial X^2}+\frac{\partial^2 V}{\partial Y^2}\right)+\mathrm{Ri}\,\theta\,\frac{(\rho\beta)_{\mathrm{nf}}}{\rho_{\mathrm{nf}}\beta_{\mathrm{f}}} \tag{10}$$

$$U\frac{\partial \theta}{\partial X}+V\frac{\partial \theta}{\partial Y}=\Omega\,\frac{\alpha_{\mathrm{nf}}}{\alpha_{\mathrm{f}}}\frac{1}{\mathrm{Re}\,\mathrm{Pr}}\left(\frac{\partial^2 \theta}{\partial X^2}+\frac{\partial^2 \theta}{\partial Y^2}\right) \tag{11}$$

where

$$\begin{cases}\lambda=\infty & \text{in solid domain}\\ \lambda=1 & \text{in fluid domain}\end{cases}\qquad \begin{cases}\Omega=\dfrac{k_{\mathrm{fin}}}{k_{\mathrm{fluid}}} & \text{in solid domain}\\ \Omega=1 & \text{in fluid domain}\end{cases}$$

In previous equations, the following non-dimensional parameters are used.

$$X=\frac{x}{W},\quad Y=\frac{y}{W},\quad U=\frac{u}{v_\infty},\quad V=\frac{v}{v_\infty},\quad P=\frac{p}{\rho_{\mathrm{nf}}\,v_\infty^{\,2}},\quad \theta=\frac{T-T_c}{T_h-T_c},$$
$$\mathrm{Re}=\frac{v_\infty W\rho_{\mathrm{f}}}{\mu_{\mathrm{f}}},\quad \mathrm{Ri}=\frac{\mathrm{Gr}}{\mathrm{Re}^2},\quad \mathrm{Gr}=\frac{g\beta_{\mathrm{f}}(T_{\mathrm{h}}-T_c)W^3}{\nu_{\mathrm{f}}^2},\quad \mathrm{Pr}=\frac{\nu_{\mathrm{f}}}{\alpha_{\mathrm{f}}} \tag{12}$$

The governing equations have elliptic nature. Therefore, boundary conditions on the entire solution domain must be specified for all field variables. The fluid enters with a uniform velocity profile. The no-slip condition is taken into account on the plate walls and surfaces of ribs (*i. e.* the nanofluid in contact with solid surfaces has the same velocity and temperature). The bottom wall has a constant temperature while the top wall is insulated. The non-dimensional boundary conditions are:

– at lower surface, including the ribs surfaces: $U = V = 0$, and $\theta = 1$,
– at the upper surface: $U = 0$, $V = -1$, $\theta = 0$ in the jet slot and $U = V = \partial\theta/\partial Y = 0.0$, otherwise,
– at $X = \pm 20$, $V = \partial\theta/\partial X = \partial Y/\partial X = 0.0$.

Nusselt number

Equating the heat transfer by convection to the heat transfer by conduction at hot wall, including the ribs surfaces and introducing the dimensionless parameters gives:

$$\mathrm{Nu}_L = \frac{h_L W}{k_\mathrm{f}} = -\frac{k_\mathrm{nf}}{k_\mathrm{f}}\left(\frac{\partial\theta}{\partial N}\right)_{N=0} \tag{13}$$

where N are the non-dimensional co-ordinates (X or Y). The average Nusselt number is obtained by integrating the local Nusselt number over the horizontal hot wall, including ribs surfaces is:

$$\mathrm{Nu} = \frac{1}{A_1 + 4A_2 + 2A_3}\int_0^{(A_1+4A_2+2A_3)} \mathrm{Nu}_L \mathrm{d}N, \quad \text{where} \quad A_1 = \frac{L-2a}{W}, \quad A_2 = \frac{b}{W}, \quad A_3 = \frac{a}{W} \tag{14}$$

Solution procedure

The governing equations were solved using the finite volume technique developed by Patankar [25]. This method was based on the discretization of the governing equations using the central difference in space. The discretization equations were solved by the Gauss-Seidel method. The iteration method employed in this program is a line-by-line procedure, which is a combination of the direct method and the resulting tri diagonal matrix algorithm (TDMA). The grid effect on the solution for average Nusselt is listed in tab. 2. The convergence of the iteration is determined by the change in the average Nusselt as well as other dependent variables through one hundred iterations to be less than 0.01% of its initial value, fig. 2.

Table 2. Grid effect on the average Nusselt number (Ri = 1, φ = 0.03, d/W = 10, and b/W = 1)

Number of grids	Nu	Number of grids	Nu
100 × 20	2.376	200 × 40	2.361
150 × 30	2.362	300 × 60	2.361

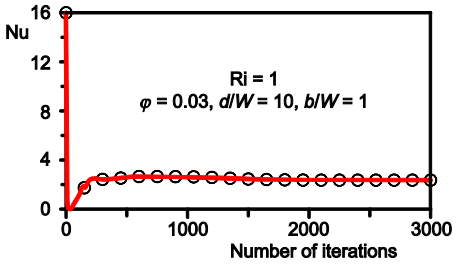

Figure 2. Convergence and stability of the solution

Program validation and comparison with previous research

The accuracy of the developed program with its numerical technique should be checked in order to be validated. Hence, it was used for the current numerical simulations.

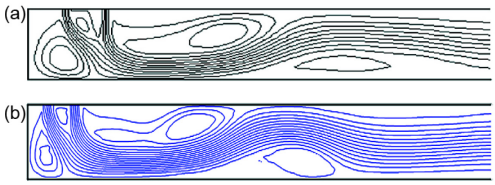

Figure 3. Stream lines for $H/W = 4$, Re = 750, and Pr = 0.7; (a) present code, (b) Dagtekin and Oztop [21]

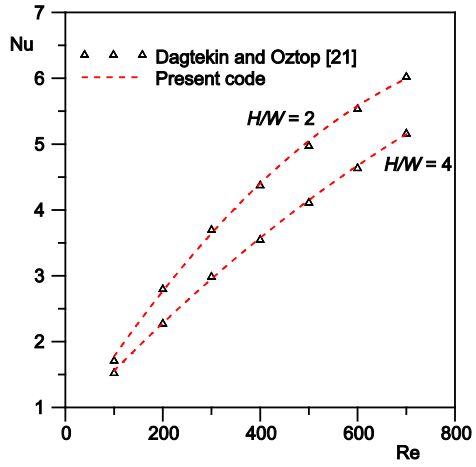

Figure 4. Average Nusselt number for Pr = 0.7

The advanced program was confirmed with Dagtekin and Oztop [21] by performing simulation for forced convection heat transfer due to double laminar slot jets impingement onto an isothermal wall within one side closed long duct. Figure 3 plots the stream lines with Pr = 0.7, H/W = 4, and Re = 750, (a) for the present code and (b) for Dagtekin and Oztop [21]. Another validation for the average Nusselt number is represented in fig. 4. The figures show good agreement between the present code and their results.

Results and discussion

After the validation of the developed code, it was used for the current simulation; the analysis of the simulated results is introduced as follows. The results include the effects of pertinent parameters such as Richardson number ($0.01 \leq$ Ri ≤ 10), the solid volume fraction ($0.01 \leq \varphi \leq 0.06$), the distance between the two ribs (d/W = 5, 10, 15) and the rib height (b/W = 1, 2, 3) on their thermal performance were introduced. The stream lines and isotherms are symmetrical about the jet location and hence the stream lines will be represented on the right-hand side while the isotherms on the left-hand side, see figs.7 and 10.

Effect of Richardson number and solid volume fraction

The effects of the Richardson number and the solid volume fraction on the heat transfer and stream lines are deliberated. Figure 5 presents the stream lines for the Cu-water nanofluid (φ = 0.01, 0.03, and 0.05) and pure water at different Richardson numbers (Ri = 0.01, 1, and 10). For both pure fluid and the nanofluid, the stream lines show that as the Richardson number decreases (forced convection domain with high inertia force of the flow) large and strong vortices are formed over the ribs. The active stream lines at low Richardson numbers enhance the heat transfer from the hot surfaces (flat surfaces and ribs). The results displayed that there is no significant difference between the stream lines of the nanofluid and pure water; this is observed from the closing of the stream line strength for both pure water and nanofluid to the same value. Nevertheless, the nanoparticles effect will be pronounced in the enhancement of nanofluid thermal conductivity. Moreover, as the solid volume fraction increases the shear stress is enhanced between the layers of the nanofluid, and that is why the vortex bulk is increased in the nanofluid. At high Richardson numbers (natural convection domain), the conduction is the dominating mechanism of heat transfer. Therefore, the strength of the stream lines became weak and stretched above the hot surfaces. There is a significant difference between the stream lines of the nanofluid and pure water; this is observed from the

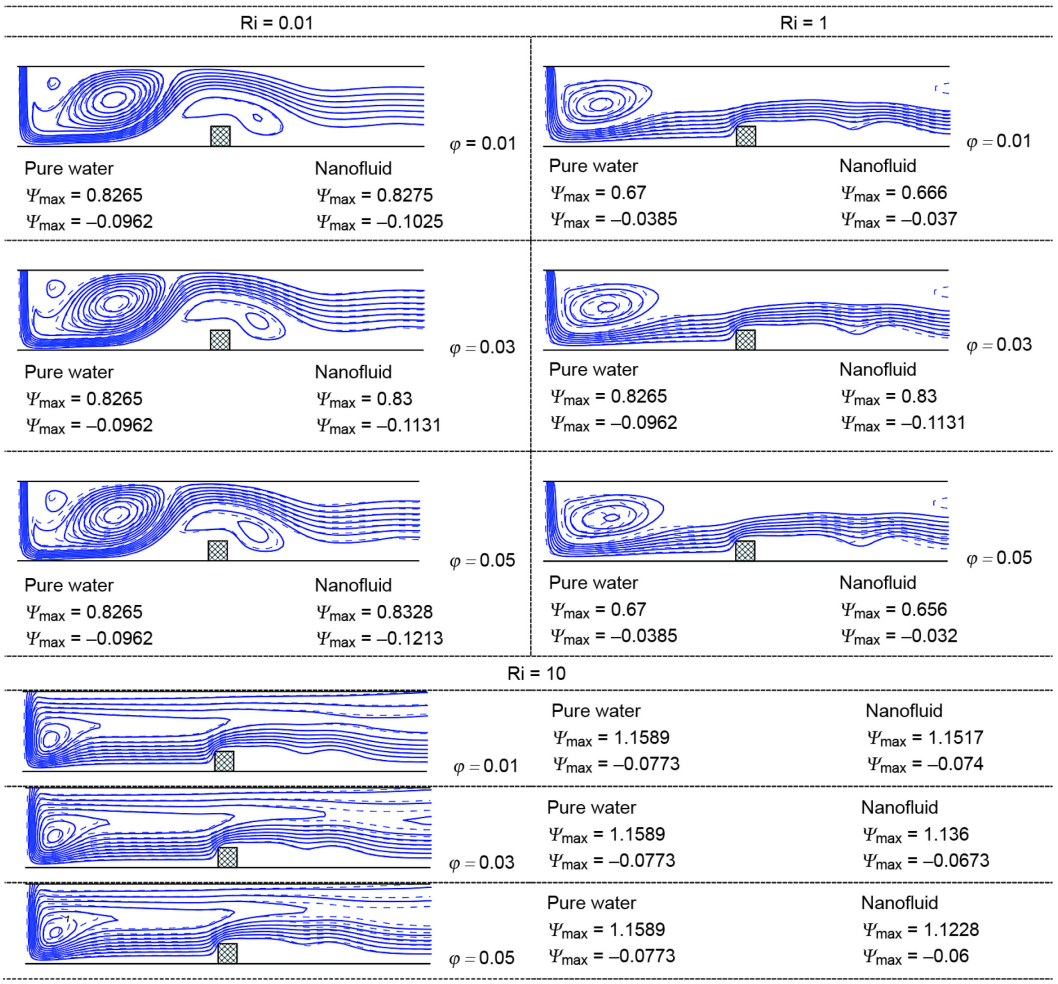

Figure 5. Stream lines for pure water (- - - -) and Cu-water nanofluid (——); $d/W = 10$, $b/W = 1$

difference of the stream line strength values for both pure water and nanofluid with higher the one being for the pure water. This is expected due to large density of the nanofluid with respect to pure water in the natural convection domain (weak driving force). This phenomenon can be explained by higher density and dynamic viscosity of the nanofluid. The effects of the solid volume fraction (φ) on the average Nusselt numbers at various Richardson numbers are studied and represented in fig. 6. For all values of the Richardson number, the average Nusselt number increases as the solid volume fraction increase (high thermal conductivity), fig. 6(a). The effects of the solid volume fraction on the average Nusselt number can be better understood by studying fig. 6(b). This figure presents the augmentation of heat transfer included in the Nusselt number values; the figure also shows that more noticeable increase in Nusselt number at low Richardson numbers where forced convection is the primary heat transfer mechanism and decreases gradually as Richardson numbers increases, this behavior due to opposite effect of both down word forced convection (nanofluid flow direction) and up word natural

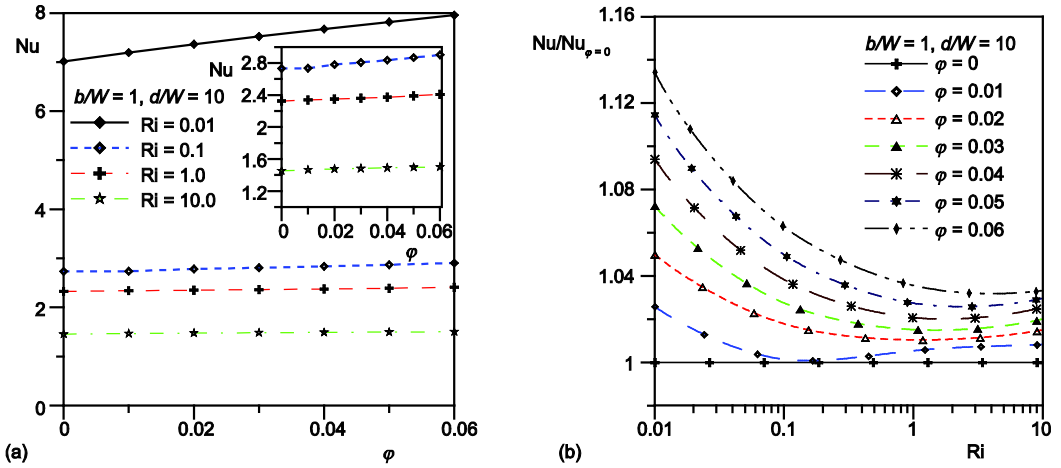

Figure 6. Average Nusselt number for different Ri and φ

convection effect in mixed convection mechanism. It's denoted that the augmentation of heat transfer slightly improved at high Richardson number due to natural convection and in the absence of forced convection.

Effect of Richardson number and rib height

The effects of both the Richardson number and the rib height on the heat transfer and the stream lines are studied. Figure 7 presents the stream lines and isotherms for the Cu-water nanofluid (φ = 0.03) for both different Richardson numbers (Ri = 0.01, 1, and 10) and different rib height (b/W = 1, 2, and 3). At small values of Richardson number (Ri = 0.01), the increasing in rib height generated a closed zone at the impingement part; this restricted area leads to the forming of larger and stronger vortices behind the rib in addition to the increase in the stream line strength. Also, a strong vortex formed before the rib, squeezing the flow near the hot surface, and this was the reason that leads to an enhancement of heat transfer. Moreover, the isotherms are closer to the hot surfaces. Consequently, a high-temperature gradient at the hot surfaces is established; this high-temperature gradient led to a high-heat transfer, especially when considering the increase in heat transfer area due to the ribs existence. As the Richardson number increases (weak flow), the generated closed zone vortex is stretched due to decreasing in the shear stress between nanofluid layers and so; the heat transfer decreases. The effects of the rib height on the average Nusselt number at various Richardson numbers are simulated and represented in fig. 8. For small values of the Richardson number, the average Nusselt number increases with the rib height increase due to the forced convection becoming dominated with strengthen vortex. The increase in rib height leads to stronger vortices, more active stream lines and closer isotherms near the hot surfaces. For weak flow, the increasing in rib height leads to decreasing in heat transfer. The stream lines strength with b/W = 1 is larger than that of b/W = 2. At low Reynolds number this phenomen can be explained by the fact that, since the inertia force of the incoming flow is weak, the effect of small rib, looks similar as for high rib. Accordingly a small strength of stream function, where b/W = 3, has a significant drop in vortices strength behind and before the rib as the Richardson number increases, this effect is shown in fig. 8(a). The effects of the existence of rib on the average Nusselt number can be better understood by studying fig. 8(b). This figure presents the amplification in heat transfer included in Nusselt

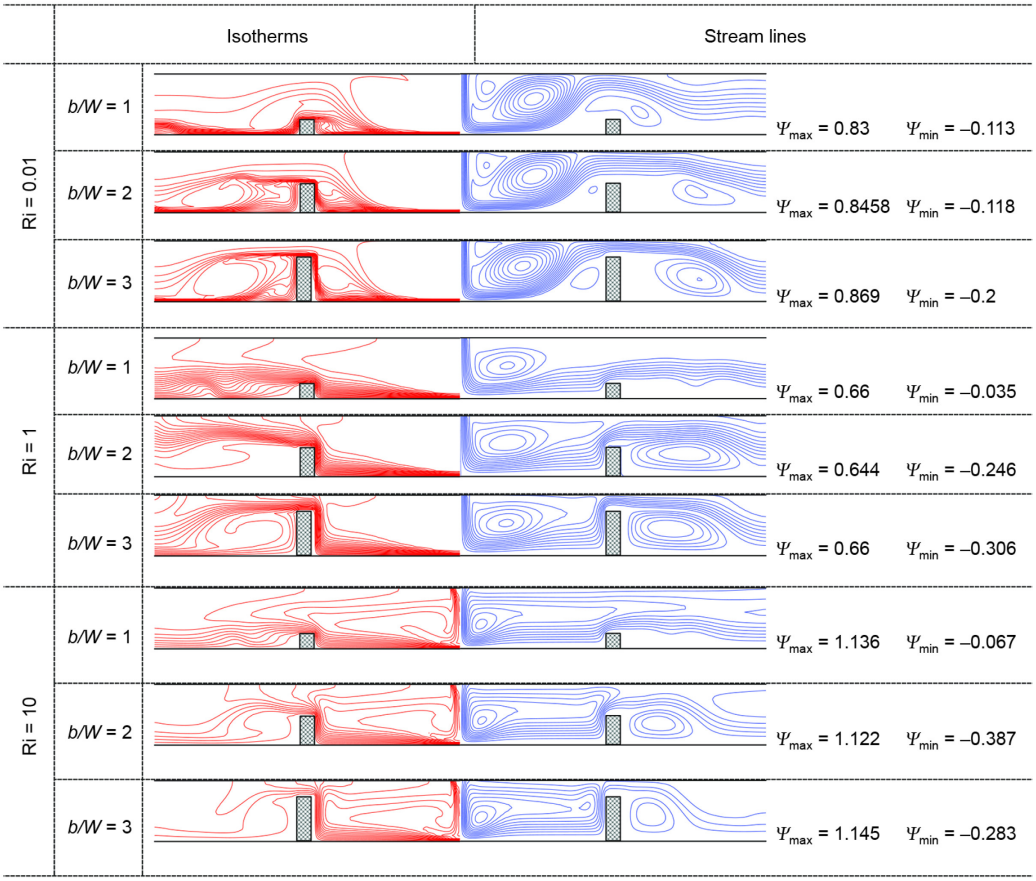

Figure 7. Stream lines (- - - -) and isotherms (——); $d/W = 10$, $\varphi = 0.03$, (Cu-water nanofluid)

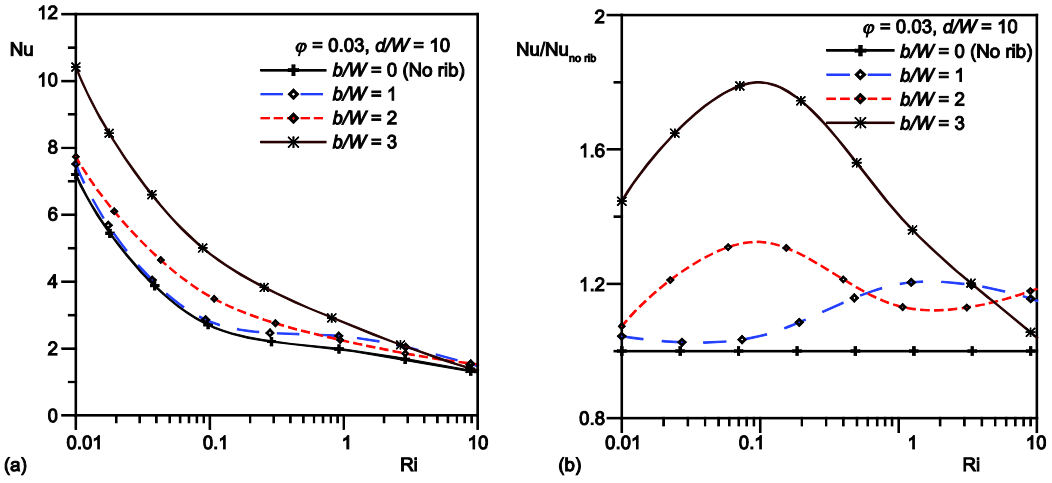

Figure 8. Average Nusselt number for different Ri and b/W

number values with respect to the existence of ribs. The figure shows that more noticeable increasing in Nusselt number due to rib existence at small Richardson numbers, and higher rib where forced convection is the primary heat transfer mechanism, but at high Richardson numbers the more elevated rib leads to decreasing in heat transfer intensity.

Effect of Richardson number and rib to a rib distance

The effects of both the Richardson number and the rib to the rib distance on the heat transfer and stream lines on the plate with ribs are studied. First, an efficient cooling with impingement jet is significant in the impingement zone. A cooling fluid with lower temperature (high-heat heat transfer rate) exists in the impingement zone. The cooling fluid temperature is increased gradually due to the escape of flow at the exit opened ports as shown in fig. 9. From the figure, the lower cooling water temperature was at $0 < X < 6$ from one side and the same from the other side, this low temperature enhanced the local Nusselt number within this zone (impingement zone), succeeding at $6 < X < 20$ the water temperature increases gradually due to absorbed heat transfer by the cooling water led to less local Nusselt number. The Richardson number values affect the increase in temperature. Consequently, it is desirable to enhance the heat transfer in this zone by squeezing the flow in this region using closer rib to rib separation distance. Figure 10 presents the stream lines and isotherms for the Cu--water nanofluid, with the concentration $\varphi = 0.03$, at different values for Richardson number, Ri = 0.01, 1, and 10. The rib to the rib distance values from the current simulation was $d/W = 5$, 10, and 15 with fixed rib height of $b/W = 1$. The Richardson number has the same effect on heat transfer as previously discussed while the effect of a rib to a rib distance on the heat transfer rate is clearly observed in the present simulation case. As the rib to rib distance decreases, closed zone at the impingement part is generated, this closed region leads to larger and stronger vortices that are formed behind the rib in addition to the increase in the stream line strength, and also, strong vortices formed before the rib squeezes the flow near the hot surface which leads to enhancement in heat transfer more than ever at low Richardson number. Also, the isotherms are closer to the hot surfaces. Therefore, the temperature gradient at the hot surfaces is high; this leads to an increase in heat transfer. In contradictory behavior, as the rib to a rib distance increases extraordinarily, the effect of this rib is an elimination of heat transfer, and exclusion of this rib will be preferable, fig. 10. It must be noted that, the perceptible enhancement in heat transfer was established at small rib to rib separation distance ($d/W = 5$), and no significant improvement in heat transfer is observed above this distance ratio.

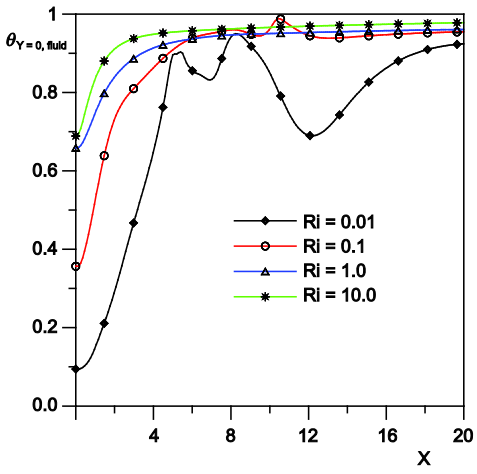

Figure 9. Local fluid temperature in contact with the bottom wall (no ribs)

Correlations for the average Nusselt number

The predicted values of average Nusselt number over the range of the investigated Richardson number and the solid volume fraction are fitted for $b/W = 1$ and $d/W = 10$, which is more applicable than the numerical values, fig. 11.

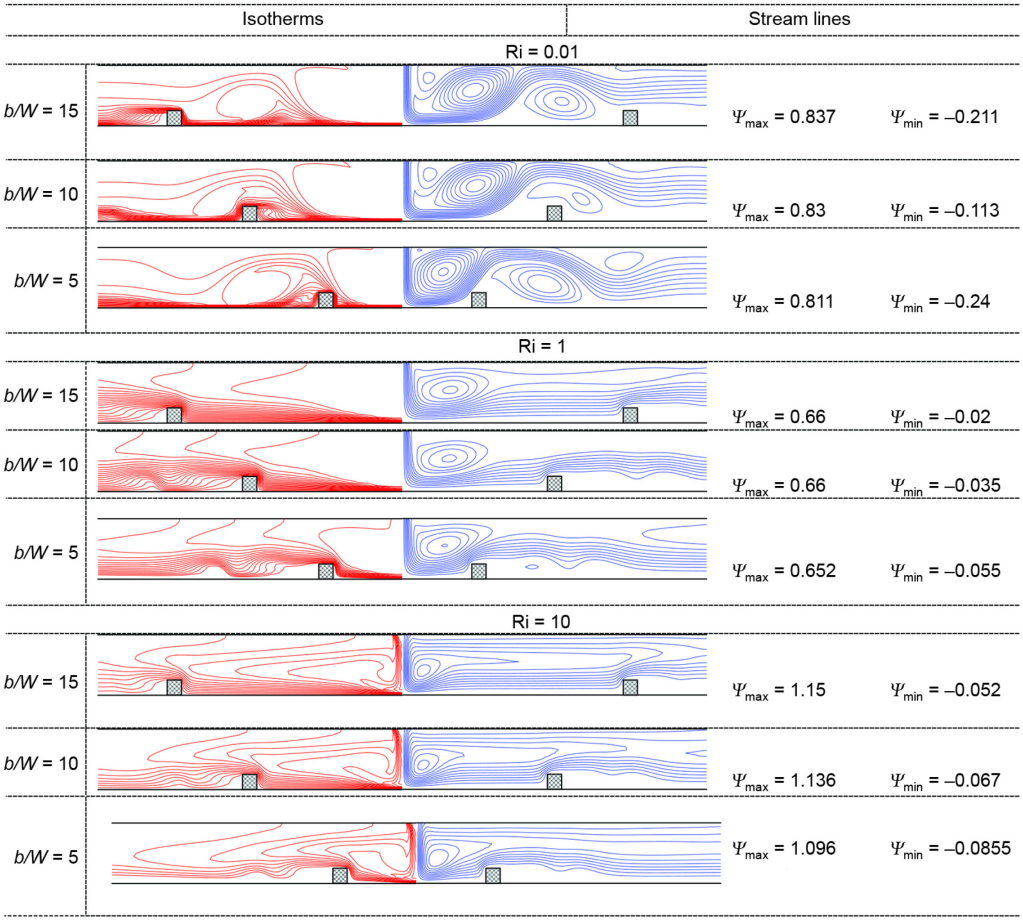

Figure 10. Stream lines (- - - -) and isotherms (——); $b/W = 1$, $\varphi = 0.03$, (water-Cu nanofluid)

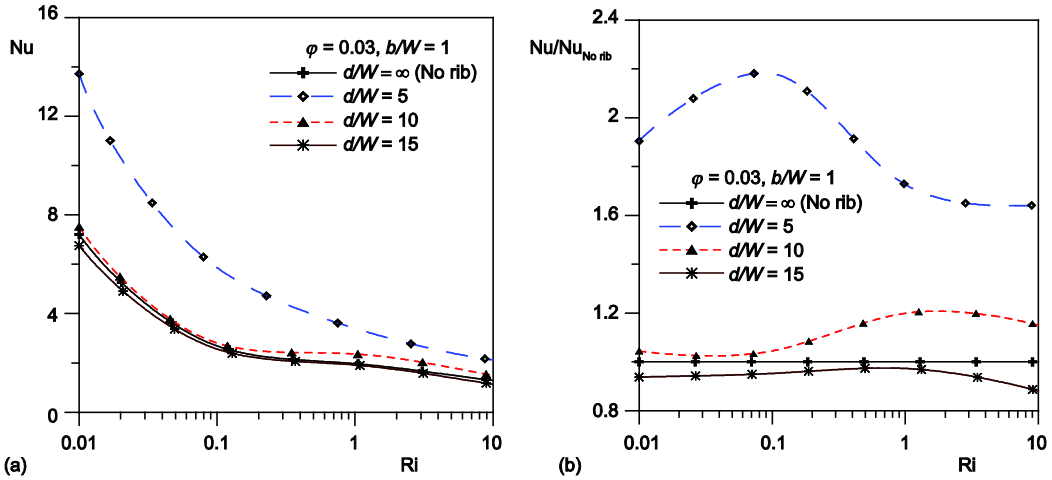

Figure 11. Average Nusselt number for different Ri and d/W

$$\mathrm{Nu} = 7.654 + 1.0775\varphi + 152.745\ \mathrm{Ri}^2 + 8.884\ \mathrm{Ri}^4 + \\ + 0.1458\ \frac{\varphi}{\mathrm{Ri}} - 63.472\ \mathrm{Ri} - 103.486\ \mathrm{Ri}^3 \tag{15}$$

with maximum deviation of 14%.

$$\frac{\mathrm{Nu}}{\mathrm{Nu}_{\varphi=0}} = 1 + 0.8738\ \varphi + 0.01422\ \frac{\varphi}{\mathrm{Ri}} + 0.034476\varphi\ \mathrm{Ri}^2 - 0.3717\varphi\ \mathrm{Ri} \tag{16}$$

with maximum deviation of 0.8%.

Conclusions

The thermal performance of two ribs mounted on the bottom wall of a horizontal flat plate is numerically simulated. The plate with ribs is cooled by Cu-water nanofluid at different nanoparticles concentrations. The simulated results are summarized as follows.

- The heat transfer rate through the plate with ribs is increased with increasing the nanoparticles concentrations. The influence of the solid volume fraction with the increase of heat transfer is more pronounced at the lower values of the Richardson number.
- The heat transfer rate is significantly affected by the distance between the ribs and the rib height.
- At low Richardson numbers (forced convection mode) the long rib (b/W) trapped the cooling water within the effective cooling zone (impingement zone) leads to heat transfer augmentation, nevertheless, at high Richardson numbers (natural convection mode) the long rib (b/W) has no noticeable effect on heat transfer due to weak flow strength.
- As the rib to a rib distance decreases, amplification of heat transfer takes place. On the other hand, as the rib to rib distance increases, the enhancement of heat transfer is not extraordinary.
- In conclusion, small Richardson number, higher rib height, nanoparticles addition and closed a rib to rib distance are essential parameters for efficient cooling.

Nomenclature

a – rib width, [m]
b – rib height, [m]
d – rib to rib distance, [m]
H – height of the duct or the jet-bottom wall spacing, [m]
h_L – heat transfer coefficient, [$\mathrm{Wm^{-2}K^{-1}}$]
k – fluid thermal conductivity, [$\mathrm{Wm^{-1}K^{-1}}$]
L – the plate length, [m]
Nu – average Nusselt number
$\mathrm{Nu_L}$ – local Nusselt number
P – dimensionless pressure, ($= p/\rho_\mathrm{f} v_\infty^2$)
Pr – Prandtl number, ($= \nu_\mathrm{f}/\alpha_\mathrm{f}$)
p – pressure, [$\mathrm{Nm^{-2}}$]
Re – Reynolds number, ($= v_\infty W/\nu_\mathrm{f}$)
Ri – Richardson number
T – local temperature, [K]
T_c – inlet fluid temperature, [K]
T_h – hot wall temperature, [K]
u – velocity components in x direction, [$\mathrm{ms^{-1}}$]
v – velocity components in y direction, [$\mathrm{ms^{-1}}$]
v_∞ – mean velocity of the jet, [$\mathrm{ms^{-1}}$]
U – dimensionless velocity component in X direction
V – dimensionless velocity component in Y direction
W – width of the jet slot, [m]
X, Y – dimensionless coordinates
x, y – dimensional coordinates

Greek symbols

α – thermal diffusivity, [$\mathrm{m^2s^{-1}}$]
β – coefficient of thermal expansion, [$\mathrm{K^{-1}}$]
θ – dimensionless temperature, $[(T - T_c)/(T_\mathrm{h} - T_c)]$
μ – dynamic viscosity, [$\mathrm{kgm^{-1}s^{-1}}$]
ν – kinematics viscosity, [$\mathrm{m^2s^{-1}}$]
ρ – local fluid density, [$\mathrm{kgm^{-3}}$]

φ – solid volume fraction
ρ – local density, [kgm^{-3}]
Ψ – stream function

Subscript

f – fluid (pure water)
nf – nanofluid
s – nanoparticle

References

[1] Maghrebi, M., *et al*., Effects of Nanoparticle Volume Fraction in Hydrodynamic and Thermal Characteristics of Forced Plane Jet, *Thermal Science, 16* (2012), 2, pp. 455-468
[2] Abdel-Fattah, A., Numerical and Experimental Study of Turbulent Impinging Twin-Jet Flow, *Experimental Thermal, and Fluid Science, 31* (2007). 8, pp.1061-1072
[3] Baydar, E., Confined Impinging Air Jet at Low Reynolds Numbers, *Experimental Thermal and Fluid Science, 19* (1999), 1, pp. 27-33
[4] Baydar, E., Ozmen, Y., An Experimental and Numerical Investigation on a Confined Impinging Air Jet at High Reynolds Numbers, *Applied Thermal Engineering, 25* (2005), 2, pp. 409-421
[5] Cavadas, A. S., *et al*., Laminar Flow Field in a Viscous Liquid Impinging Jet Confined by Inclined Plane Walls, *International Journal of Thermal Sciences, 59* (2012a), Sep., pp. 95-110
[6] Choo, K. S., Kim, S. J., Comparison of Thermal Characteristics of Confined and Unconfined impinging Jets, *International Journal of Heat and Mass Transfer*, *53* (2010), 15, pp. 3366-3371
[7] Guerra, D. R. S., *et al*., The Near Wall Behavior of an Impinging Jet, *International Journal of Heat and Mass Transfer, 48* (2005), 14, pp. 2829-2840
[8] Koseoglu, M. F., Baskaya, S., Experimental and Numerical Investigation of Natural Convection Effects on Confined Impinging Jet Heat Transfer, *International Journal of Heat and Mass Transfer, 52* (2009), 5, pp. 1326-1336
[9] Lee, D. H., *et al*., Confined, Milliscale Unsteady Laminar Impinging Slot Jets and Surface Nusselt Numbers, *International Journal of Heat and Mass Transfer, 54* (2011), 11, pp. 2408-2418
[10] Lee, H. G., *et al*., A Numerical Investigation on the Fluid Flow and Heat Transfer in the Confined Impinging Slot Jet in the Low Reynolds Number Region for Different Channel Heights, *International Journal of Heat and Mass Transfer, 51* (2008), 15, pp. 4055-4068
[11] Nguyen, C. T., *et al*., An Experimental Study of a Confined and Submerged Impinging Jet Heat Transfer Using Al_2O_3-Water Nanofluid, *International Journal of Thermal Sciences, 48* (2009), 2, pp. 401-411
[12] Ozmen, Y., Confined Impinging Twin Air Jets at High Reynolds Numbers, *Experimental Thermal and Fluid Science, 35* (2011), 2, pp. 355-363
[13] San, J.-Y., Chen, J.-J., Effects of Jet-to-Jet Spacing and Jet Height on Heat Transfer Characteristics of an Impinging Jet Array, *International Journal of Heat and Mass Transfer, 71* (2014), Apr., pp. 8-17
[14] San, J.-Y., Shiao, W.-Z., Effects of Jet Plate Size and Plate Spacing on the Stagnation Nusselt Number for a Confined Circular Air Jet Impinging on a Flat Surface, *International Journal of Heat and Mass Transfer, 49* (2006), 19, pp. 3477-3486
[15] Yousefi-Lafouraki, B., *et al*., Laminar Forced Convection of a Confined Slot Impinging Jet in a Converging Channel, *International Journal of Thermal Sciences, 77* (2014), Mar., pp. 130-138
[16] Zukowski, M., Heat Transfer Performance of a Confined Single Slot Jet of Air Impinging on a Flat Surface, *International Journal of Heat and Mass Transfer, 57* (2013), 2, pp. 484-490
[17] Behnia, M., *et al*., Numerical Study of Turbulent Heat Transfer in Confined and Unconfined Impinging Jets, *International Journal of Heat and Fluid Flow, 20* (1999), 1, pp. 1-9
[18] Beitelmal, A. H., *et al*., The Effect of Inclination on the Heat Transfer between a Flat Surface and an Impinging Two-Dimensional Air Jet, *International Journal of Heat and Fluid Flow, 21* (2000), 2, pp. 156-163
[19] Senter, J., Solliec, C., Flow Field Analysis of a Turbulent Slot Air Jet Impinging on a Moving Flat Surface, *International Journal of Heat and Fluid Flow, 28* (2007), 4, pp. 708-719
[20] Yan, X., Saniei, N., Heat Transfer from an Obliquely Impinging Circular, Air Jet to a Flat Plate, *International Journal of Heat and Fluid Flow, 18* (1997), 6, pp. 591-599
[21] Dagtekin, I., Oztop, H. F., Heat Transfer Due to Double Laminar Slot Jets Impingement onto an Isothermal Wall within One Side Closed Long Duct, *International Communications in Heat and Mass Transfer, 35* (2008), 1, pp. 65-75
[22] Brinkman, H. C., The Viscosity of Concentrated Suspensions and Solution, *J. Chem. Phys., 20* (1952), 4, pp. 571-581

[23] Patel, H. E., *et al*., A Micro-Convection Model for Thermal Conductivity of Nanofluids, *Pramana, J. Phys., 65* (2005), 5, pp. 863-869
[24] Santra, A. K., *et al*., Study of Heat Transfer Due to Laminar Flow of Copper-Water Nanofluid Through Two Isothermally Heated Parallel Plates, *Int. J. Therm. Sci., 48* (2009), 2, pp. 391-400
[25] Patankar, S., *Numerical Heat Transfer and Fluid Flow*, McGraw-Hill, New York, USA, 1980

Paper submitted: December 28, 2014
Paper revised: March 9, 2015
Paper accepted: Apryl 3, 2015